



Computational Study Using Tight-Binding Propagation Method: Optical Properties of Defected WS_2 Monolayer

I Wayan Windu Sara^{1,a} and I Gede Arjana²

¹Department of Physics, Universitas Jember, Jember, Indonesia

²Department of Physics, Universitas Pendidikan Ganesha, Bali, Indonesia

^awyn.windu@unej.ac.id

Abstract. *Materials computing is the interdisciplinary science of designing and investigating materials and their intrinsic properties through computational approaches. One promising material in the class of Transition Metal Dichalcogenides (TMDCs) is the monolayer of tungsten disulfide (WS_2), which has shown significant potential for applications in optoelectronics, including solar cell technology. While various experimental and theoretical studies have explored the optical properties of WS_2 monolayers, most have focused only on pristine structures or limited defect types. In this study, we investigate the influence of vacancy defects—specifically, different types and concentrations ranging from 1% to 5%—on the optical properties of WS_2 monolayers using the tight-binding propagation method implemented via the TBPLaS computational library. Our results show that both the type and concentration of vacancies significantly alter the absorption spectra and optical transitions, with distinct effects observed across different energy ranges. The presence of defects generally reduces optical performance in the visible range, potentially limiting solar cell efficiency. However, the defect-induced modifications in the infrared region suggest a new potential for WS_2 monolayers in infrared sensing applications.*

Keywords: Tight binding, propagation method, WS_2 monolayer, vacancies, optical properties

Introduction

Semiconductor is one type of material that plays an important role in the progress of human civilization to the present [1]. Although there are many types, semiconductor materials such as silicon are widely used in modern technology because of their abundant availability and good performance in technological applications [2]. One important silicon-based technology is solar cells, which convert solar energy into electrical energy [3]. Solar cell technology offers an alternative mechanism to meet the need for clean, low-emission, and environmentally friendly energy [4]. Because of this potential, a lot of research and development has been done to improve the performance and portability of solar cells [5], [6].

One of the efforts to improve the performance of solar cells is to integrate a Tungsten Disulfide (WS_2) layer as an electron transport layer [7]. WS_2 is one type of semiconductor material that belongs to Transition Metal Dichalcogenides (TMDC) [8]. In addition, the WS_2 layer also has the potential to be applied as an absorber layer on solar cells to increase their efficiency [9]. In another study, a single layer of WS_2 can increase absorption in the visible light region when applied as an intermediate layer on hetero-structure-based solar cells [10]. Even single-layer WS_2 itself has been developed as a transparent solar cell [11].

However, the synthesis process or environmental factors can cause the WS_2 monolayer to experience internal defects such as vacancies, potentially reducing its performance as an integrated layer in solar cells [12]. In addition to vacancies, WS_2 monolayers also have the opportunity to oxidize due to their interaction with free air [13]. The type of vacancies of W atoms

or S atoms in WS_2 monolayers is thought to affect its optical properties [14]. Moreover, the presence of vacancies also has an impact on changes in the density of states and energy band gap of WS_2 monolayers [15].

Several studies have been conducted to study the optical character of WS_2 monolayer in its pristine state as well as in the presence of atomic defects such as vacancies using Density Functional Theory (DFT) [14], [16], [17]. However, the concentration of vacancies studied using the DFT method is relatively not low enough due to its expensive computation cost [18]. In DFT, for lower vacancies, a larger system size is required and this leads to an increase in the amount of memory required up to ~100 GB [19]. As an alternative, a method that can be obtained is the tight binding propagation method [20]. This method has been used to study and predict the electrical and optical characteristics of two-dimensional TMDC materials with relatively very low vacancy concentration at a relatively affordable computational cost [21].

Current computational studies of the optical properties of WS_2 monolayer are still limited to variations in the concentration of vacancies that are large enough or very small so that they do not provide a comprehensive picture or prediction related to the effect of vacancy concentration on the optical properties of materials [17], [18], [21]. Therefore, this research studies the effect of the presence of W, S₂, and WS_2 vacancies ranging from 1-5% that may happen in WS_2 monolayer on its optical properties. The calculated optical properties such as optical conductivity, refractive index, reflectance, and absorption coefficient are quantities that can describe the behavior of materials due to interaction with light as electromagnetic waves. The study in this research is carried out computationally using the TBPLaS library as an implementation of the tight binding propagation method.

Theoretical Background

The structure and Hamiltonian of WS_2 monolayer are important concepts for calculating optical properties in tight binding propagation simulations.

Structure and tight binding Hamiltonian of WS_2

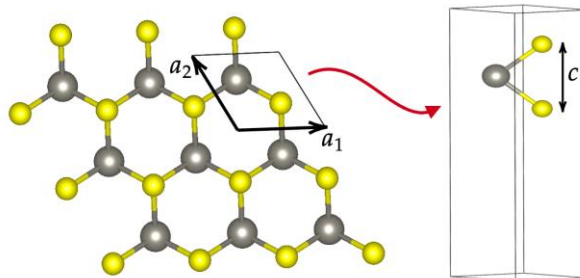


Figure 1. Hexagonal structure of WS_2 monolayer and unit cell of WS_2 monolayer consists of one W atom & two S atoms

WS_2 monolayer is a two-dimensional material consisting of a layer of Tungsten W atoms sandwiched by two layers of Sulfur S atoms [22]. The structure of the WS_2 layer is similar to the hexagonal structure of graphene, but the unit cell contains one W atom and two S atoms [23]. The lattice parameter of the WS_2 monolayer structure $a = 3,18 \text{ \AA}$ [24]. While, the closest distance

between S atoms in one unit cell is $c = 3,142 \text{ \AA}$ [25]. In the representation of the crystal system, the lattice vectors of single-layer WS₂ are expressed as $a_1 = (a, 0, 0)$ dan $a_2 = (-\frac{a}{2}, \frac{a\sqrt{3}}{2}, 0)$ as shown in **Figure 1**.

The tight binding method uses a linear combination of atomic orbitals as an orthogonal basis state in solving the time-independent Schrödinger equation [26]. For WS₂ monolayer, W atom and 2 S atoms in each unit cell can respectively contribute atomic orbitals $\{d_{3z^2-r^2}, d_{x^2-y^2}, d_{xy}, d_{xz}, d_{yz}\}$ and $\{p_x, p_y, p_z\}$ thus the orthogonal basis consists of 11 orbitals, namely $|\phi_i\rangle = |p_{i,x,t}, p_{i,y,t}, p_{i,z,t}, d_{i,3z^2-r^2}, d_{i,x^2-y^2}, d_{i,xy}, d_{i,xz}, d_{i,yz}, p_{i,x,b}, p_{i,x,b}, p_{i,x,b}\rangle$ [27]. The index i represents the unit cell number, while t and b indicate the orbitals of the upper S and lower S atoms, respectively. In the second quantization using the on-site parameter $\epsilon_i = \langle \phi_i | -\frac{\hbar^2}{8\pi^2 m} \nabla^2 + V(r) | \phi_i \rangle$ and the hopping parameter between orbitals i & j $t_{ij}(\mathbf{R}) = -\langle \phi_i(\mathbf{0}) | -\frac{\hbar^2}{8\pi^2 m} \nabla^2 + V(r) | \phi_j(\mathbf{R}) \rangle$, the Hamiltonian matrix of single layer WS₂ in real space can be expressed as [28]:

$$\hat{H} = \sum_{\mathbf{R}, i} \epsilon_i c_i^\dagger(\mathbf{R}) c_i(\mathbf{R}) + \sum_{\mathbf{R} \neq \mathbf{0} \forall i \neq j} t_{ij}(\mathbf{R}) c_i^\dagger(\mathbf{0}) c_j(\mathbf{R}) \quad (1)$$

where c^\dagger and c are the creation and annihilation operators respectively in the basis used. While, \mathbf{R} represents the unit cell position. The tight-binding parameters for the WS₂ monolayer used refer to previous work [27]. The complete solution of the Schrödinger equation using the Hamiltonian as equation (1) can be expressed by $|\psi(t)\rangle = e^{-i\hat{H}t} |\psi(0)\rangle$, where $|\psi(0)\rangle$ consists normalized initial random states in all basis $|\phi_i\rangle$ in the sample [29]. The time exponential term is approximated using Chebyshev polynomials as follows $e^{-i\hat{H}t} = e^{-i(\frac{\hat{H}}{\|\hat{H}\|})(\|\hat{H}\|t)} = e^{-i\hat{H}\tilde{t}} = [J_0(\tilde{t})\hat{T}_0(\tilde{H}) + 2J_1(\tilde{t})\hat{T}_1(\tilde{H}) + 2\sum_{m=2}^{\infty} J_m(\tilde{t})\hat{T}_m(\tilde{H})]$ where $J_m(\tilde{t})$ is the Bessel function and $\hat{T}_m(\tilde{H})$ is the modified Chebyshev polynomials that has iteration $\hat{T}_{m+1}(\tilde{H}) = -2i\tilde{H}\hat{T}_m(\tilde{H}) + \hat{T}_{m-1}(\tilde{H})$ with the generators $\hat{T}_0(\tilde{H}) = I$ and $\hat{T}_1(\tilde{H}) = -i\tilde{H}$ [28]. Use of Chebyshev polynomials to avoid impractical diagonalization of the sparse Hamiltonian matrix or the 4th order Runge-Kutta method which requires small time steps to produce good results [30].

Optical Properties: Optical Conductivity, refractive index, Reflectance, and Absorption Coefficient

Optical conductivity is the response of a material to electromagnetic waves [31]. Based on Kubo's formula, the real part of the optical conductivity of a sample of size Ω in the same direction as the direction of electromagnetic wave can be expressed as [32]

$$Re \sigma_{xx}(\hbar\omega) = \lim_{E \rightarrow 0^+} \frac{e\beta\hbar\omega - 1}{\hbar\omega\Omega} \int_0^\infty e^{-Et} \sin(\omega t) \times [2Im\langle \psi_2(t) | J_x | \psi_1(t) \rangle_x] dt \quad (2)$$

with $|\psi_2(t)\rangle = e^{-i\hat{H}\tilde{t}} f(\tilde{H}) |\psi(0)\rangle$ dan $|\psi_1(t)\rangle_x = e^{-i\hat{H}\tilde{t}} [1 - f(\tilde{H})] J_x |\psi(0)\rangle$. Current density operator is denoted by $J_x = -\frac{ie}{\hbar} \sum_{i,j} t_{ij} (\hat{r}_j - \hat{r}_i)_x c_i^\dagger c_j$ with $(\hat{r}_j - \hat{r}_i)_x$ is x-direction component of position operator & e is electron charge, meanwhile Fermi-Dirac distribution operator approximated using Chebyshev polynomial $f(\tilde{H}) = \sum_{k=0}^{\infty} c_k T_k(\tilde{H})$, c_k is Chebyshev expansion coefficient of the

function $f(\tilde{H}) = (e^{\beta\mu})(e^{-\tilde{\beta}\tilde{H}})/(1 + (e^{\beta\mu})(e^{-\tilde{\beta}\tilde{H}}))$ and calculated using fast Fourier transform & $T_k(\tilde{H})$ is the modified Chebyshev polynomials that has iteration $T_{k+1}(\tilde{H}) - 2\tilde{H}T_k(\tilde{H}) + T_{k-1}(\tilde{H}) = 0$ with the generators $T_0(\tilde{H}) = 1$ and $T_1(\tilde{H}) = \tilde{H}$ [29]. The imaginary part of the optical conductivity can be obtained from the Kramers-Kronig relation as [28]

$$Im \sigma_{xx}(\hbar\omega) = -\frac{1}{\pi} \mathcal{P} \int_{-\infty}^{\infty} \frac{\sigma_{xx}(\hbar\omega')}{\omega' - \omega} d\omega' \quad (3)$$

where \mathcal{P} represents the Cauchy principal part of the integration. The real and imaginary parts of the optical conductivity $Re \sigma_{xx}$ and $Im \sigma_{xx}$ can provide information regarding the complex value of the relevant dielectric constant $\epsilon(\omega) = \epsilon_1(\omega) + i\epsilon_2(\omega)$ based on the formulas $\epsilon_1 = \frac{Im \sigma_{xx}}{\omega\epsilon_0}$ and $\epsilon_2 = \frac{Re \sigma_{xx}}{\omega\epsilon_0}$ [33]. The real and imaginary values of the dielectric constants are then used to calculate optical properties such as refractive index $n(\omega)$, reflectance $R(\omega)$, and absorption coefficient $\alpha(\omega)$ respectively using the following formulas [34].

$$n(\omega) = \sqrt{\frac{|\epsilon(\omega)| + Re(\epsilon(\omega))}{2}} \quad (4)$$

$$R(\omega) = \frac{(n(\omega) - 1)^2 + \kappa(\omega)^2}{(n(\omega) + 1)^2 + \kappa(\omega)^2} \quad (5)$$

$$\alpha(\omega) = \frac{2\omega\kappa(\omega)}{c} \quad (6)$$

where $\kappa(\omega) = \sqrt{\frac{|\epsilon(\omega)| - Re(\epsilon(\omega))}{2}}$.

Materials and Methods

This research utilizes a personal computer with an Intel core i5-13420H processor (12 CPUs, ~2.1 GHz), 16 GB RAM (4267 MT/s), and a Linux-based operating system, Pop!_OS. During the calculation process, the computer was operated remotely using tunneling available in VSCode software.

This work is based on a tight binding model that is computed using the time propagation method. The method is used because it can produce a time-dependent Schrödinger equation solution of a large system without going through the diagonalization process, which is relatively expensive [28]. This study implements an open-source library TBPLaS, which is a library that integrates the time propagation method to study large systems based on the tight binding model [28].

The considered WS₂ monolayer system has a size of 100 × 100 thus contains 30.000 atoms and 110.000 atomic orbitals. This size is relatively convergent in showing the physical profile of the WS₂ monolayer so that it is considered to represent the real WS₂ monolayer [15]. At first, the calculation of optical properties such as optical conductivity, refractive index, reflectance, and absorption coefficient is applied to the pristine system without the presence of vacancies. Furthermore, similar calculations were applied to a system of the same size, but with the presence of 3 types of vacancy defects, namely atomic vacancy defects W, S₂, and WS₂ with concentration variations from 1%, 2%, 3%, 4%, and 5%. The three types of vacancies are shown in **Figure 2**.

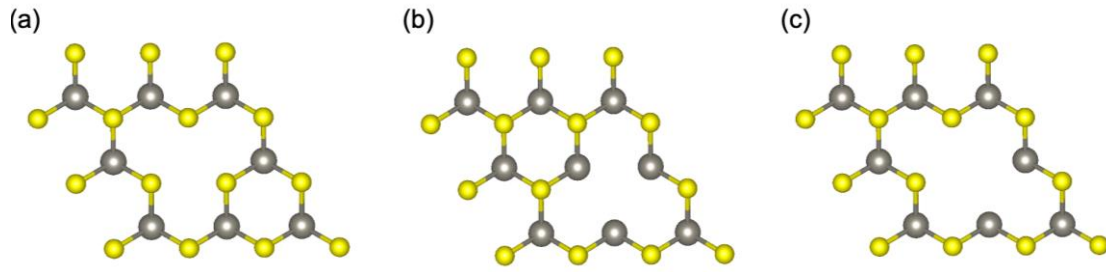


Figure 2. WS₂ monolayer with: (a) vacancy of W atom, (b) vacancy of S₂ atom, and (c) vacancy of WS₂ atom

Results and Discussion

A computational study of the optical properties of WS₂ monolayers with variations of W, S₂, and WS₂ atomic vacancies in the same unit cell has been conducted. The position of each vacancy is generated using a random number generator to represent the real system condition. The concentration of applied vacancies varies from 1-5% to study the effect of vacancies on the optical properties of WS₂ monolayers. The study of optical properties was carried out in the infrared to a small part of the ultraviolet energy range (0 or 1 - 5eV) because the solar energy spectrum is mostly dominated by infrared and visible light [35].

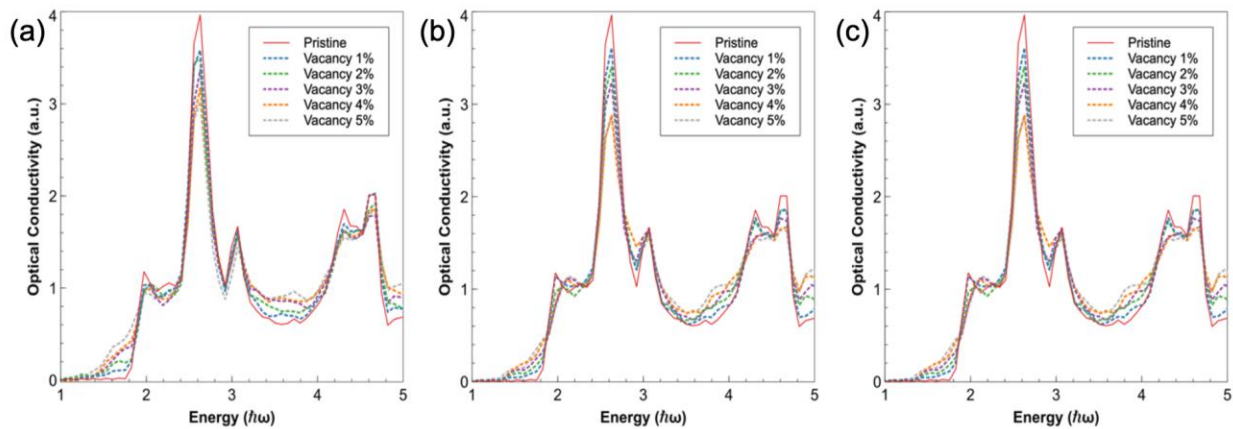


Figure 3. Optical conductivity of WS₂ monolayer with varying vacancy: (a) vacancy of W atom, (b) vacancy of S₂ atom, and (c) vacancy of WS₂ atom

Based on **Figure 3**, in the energy range of 1-2 eV, all types of atomic vacancies with a vacancy concentration of 1-5% tend to increase the optical conductivity of WS₂ monolayer. The same is observed around energies of 3,2 - 4,2 eV and 4,8 eV. This is thought to be due to a decrease in the energy band gap around 1-2 eV due to changes in state localization [15], while other energy regions are thought to be due to momentum transfer from photons to charge carriers [36]. Meanwhile, in other energy regions there is a decrease in optical conductivity due to system irregularities that interfere with the transportation of charge carriers with a certain momentum [37]. Although the peaks of optical conductivity values around 2 eV, 2.7 eV, 3.1 eV, 4.3 eV, and 4.6 eV tend to decrease, the other energy regions increase. In general, this has a good impact on charge

carrier transport in WS₂ monolayers applied to solar cells, given the broad spectrum of sunlight. On closer inspection, **Figure 3 (a)** shows a more significant increase in the non-peak region compared to others and a smaller decrease in the peak region in the 1 - 4eV energy range. This indicates that the presence of W atomic vacancies is relatively superior in maintaining and enhancing optical conductivity compared to S₂ or WS₂ type vacancies. This finding also indicates that WS₂ monolayer with variations in the type and number of vacancies can be applied to the field of light sensors in specific spectral ranges, especially infrared and red color.

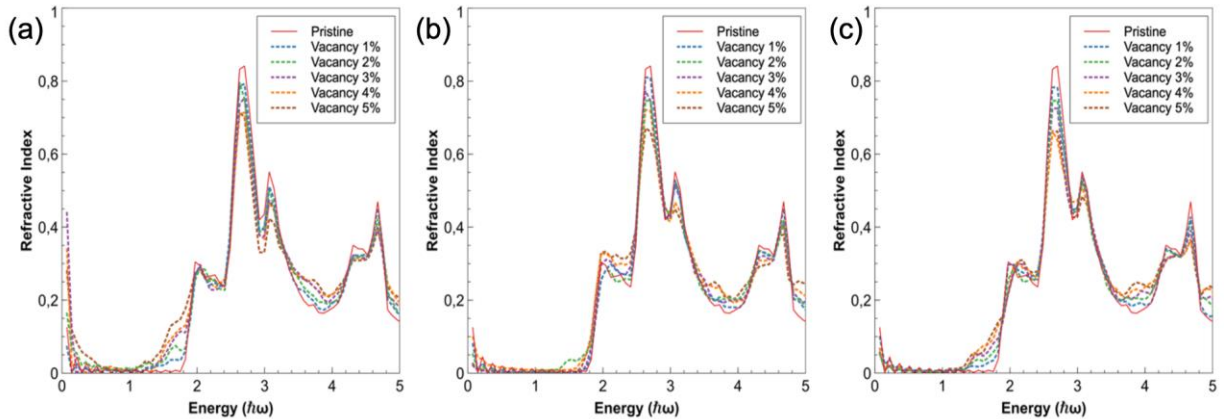


Figure 4. Refractive index of WS₂ monolayer with varying vacancy: (a) vacancy of W atom, (b) vacancy of S₂ atom, and (c) vacancy of WS₂ atom

The refractive index of the WS₂ monolayer system was calculated from the optical conductivity data obtained previously. In general, **Figure 4** shows that the refractive index of the WS₂ monolayer depends on the energy of the electromagnetic waves passing through it. At low energy levels between 0.2 - 1 eV, electromagnetic waves experience relatively little refraction because they pass through systems with minimal energy or momentum transfer. Meanwhile, in the energy region of more than 1 eV, it appears to depend on the type and number of vacancies of the atoms that make up the WS₂ monolayer. This is related to the mechanism in optical conductivity previously discussed. In the energy range of 1-2 eV, the refractive index of WS₂ monolayers subjected to W-type vacancies increases as the concentration increases (**Figure 4(a)**), but this is not the case for WS₂ monolayers subjected to S₂ and WS₂ atomic vacancies (**Figure 4(b)** and **(c)**). For the region around energy 2 - 2.4 eV, increasing the concentration of S₂ atomic vacancies from 3 - 5% can increase the refractive index of the system. The same thing happens in WS₂ monolayer with WS₂ vacancies, but not as significant as that in WS₂ monolayer with S₂ vacancies. On the other hand, the WS₂ monolayer with W atom vacancies shows a decrease in refractive index. Other than at 2 eV energy, the dominant peaks decrease. This indicates that the presence of vacancies with various types and concentrations can reduce the refractive index at certain energy levels. Meanwhile, the non-peak regions experience an increase in refractive index. The greater the refractive index, the greater the ability of the material to trap light with certain energies. This opens up the potential to make solar cells more compact.

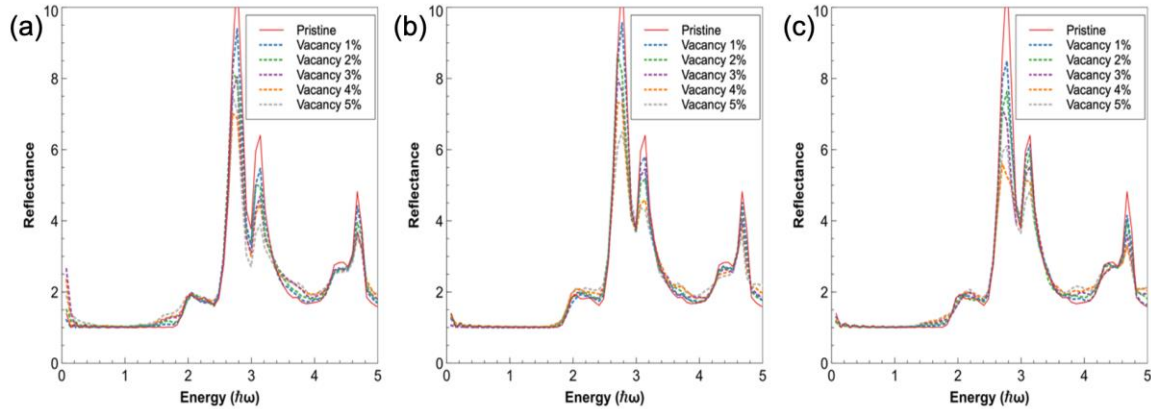


Figure 5. Reflectance of WS_2 monolayer with varying vacancy: (a) vacancy of W atom, (b) vacancy of S_2 atom, and (c) vacancy of WS_2 atom

Reflectance describes how a material reflects back electromagnetic waves that hit it. Visualization of the reflectance of the WS_2 monolayer in this study is presented in **Figure 5**. Similar to the optical properties previously discussed, reflectance also depends on the type of electromagnetic wave spectrum that hits it. Electromagnetic waves with energy greater than 2 eV tend to be reflected more than electromagnetic waves with smaller energy. This is related to the number of charge carriers localized at a certain energy level. The more charges that are localized at an energy level, the greater the reflectance. Vacancy of W, S_2 , and WS_2 atoms causes a change in the localization of charge carriers resulting in a change in reflectance [38]. The WS_2 monolayer with W atomic vacancies (**Figure 5(a)**) results in a larger reflectance enhancement than that exhibited by the WS_2 monolayer with WS_2 atomic vacancy in the energy range of 1 - 2 eV. The similar situation is not significant for WS_2 monolayer with S_2 atomic vacancies. In **Figure 5 (a) - (c)** there are three dominant peaks that have reduced reflectance. The larger reduction in reflectance due to the increase in vacancy concentration is only shown by WS_2 monolayer with S_2 vacancies in the energy range of about 2,8 eV and WS_2 monolayer with W or WS_2 vacancies in the energy range of about 3,2 eV. Meanwhile, the non-peak regions generally experience an increase in reflectance. This finding indicates a reduction in the performance of the WS_2 monolayer containing vacancies as it reflects more of the dominant sun light spectrum.

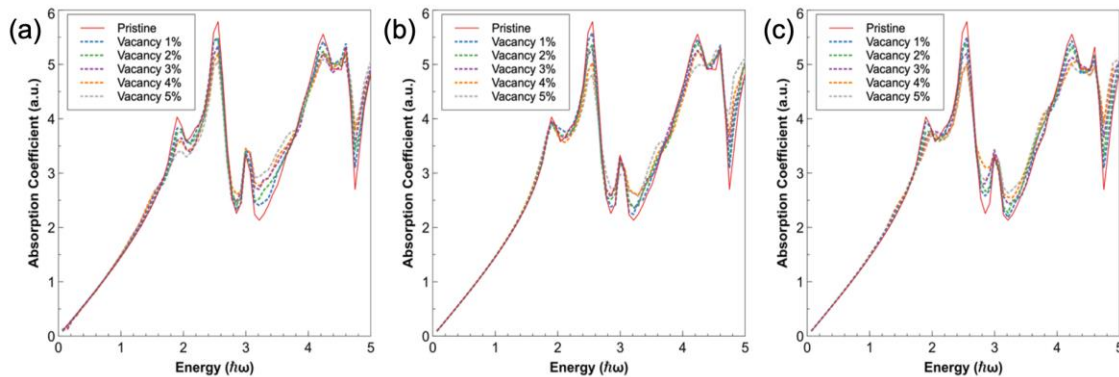


Figure 6. Absorption coefficient of WS_2 monolayer with varying vacancy: (a) vacancy of W atom, (b) vacancy of S_2 atom, and (c) vacancy of WS_2 atom



Electromagnetic waves that are not reflected will then undergo two processes: absorption and transmission. Electron will use the energy from the absorbed wave spectrum to transition to a higher energy level. This is the main working principle of solar cells. **Figure 6** shows that the absorption coefficient tends to be linear at low levels of the energy spectrum. Furthermore, at relatively high energy levels the value is highly dependent on the electromagnetic wave spectrum. The presence of vacancies, both W, S₂, and WS₂ atoms, shows a tendency to decrease the absorption coefficient around the energy region of 1,8 - 2,6 eV. The reduction of the absorption coefficient also occurs in the region around energy 4.2 eV. The reason is that the population of charge carriers localized at that energy is largely reduced. An increase in the concentration of vacancies that decreases the absorption coefficient is only clearly observed in the WS₂ monolayer with S₂ vacancies in the energy range around ~2.5 eV in **Figure 6 (b)**. Meanwhile, the absorption coefficient in some energy ranges increases. However, the power per unit area of sunlight reaching Earth is relatively smaller for photon energies higher than 3 eV [35] [39]. Ultimately, this results in a decrease in the performance of solar cells based on WS₂ monolayers due to the reduction of the absorption coefficient in the dominant region of the sunlight spectrum.

Conclusions

Calculation of the optical properties of WS₂ monolayer was successfully carried out using TBPLaS based on tight binding propagation. The optical properties studied include optical conductivity, refractive index, reflectance, and absorption coefficient. The calculations show a change in optical properties when the WS₂ monolayer is subjected to W, S₂, and WS₂ type vacancies with concentrations of 1-5%. In certain energy regions, the four optical properties studied increased or decreased. This is related to changes in the localization of charge carriers in the WS₂ monolayer due to the different types and variations in the concentration of the vacancy defects. The change in optical properties tends to make the performance of WS₂ monolayer decrease when applied as an absorber in solar cells. For the future, further research can be carried out by studying the effect of the presence of W, S₂, and WS₂ atomic vacancies simultaneously on a WS₂ monolayer system which is not discussed in this research.

References

- [1] Z. Qiu, X. Shen, and Z. Zhao, "Development Trends and Prospects of Semiconductor Devices and Technology," 2024.
- [2] J. Song, "The history and trends of semiconductor materials' development," in *Journal of Physics: Conference Series*, Institute of Physics, 2023. doi: 10.1088/1742-6596/2608/1/012019.
- [3] A. S. Al-Ezzi and M. N. M. Ansari, "Photovoltaic Solar Cells: A Review," Aug. 01, 2022, *MDPI*. doi: 10.3390/asi5040067.
- [4] G. T. Chala and S. M. Al Alshaikh, "Solar Photovoltaic Energy as a Promising Enhanced Share of Clean Energy Sources in the Future—A Comprehensive Review," Dec. 01, 2023, *Multidisciplinary Digital Publishing Institute (MDPI)*. doi: 10.3390/en16247919.



-
- [5] Shreya, P. Phogat, R. Jha, and S. Singh, "Emerging advances and future prospects of two dimensional nanomaterials based solar cells," Oct. 05, 2024, *Elsevier Ltd.* doi: 10.1016/j.jallcom.2024.175063.
- [6] T. Younas, U. A. Khan, S. M. F. H. Zaidi, and M. H. Khalid, "Increasing Efficiency of Solar Panels via Photovoltaic Materials," in *IOP Conference Series: Earth and Environmental Science*, Institute of Physics, 2022. doi: 10.1088/1755-1315/1048/1/012005.
- [7] M. F. Rahman *et al.*, "Concurrent investigation of antimony chalcogenide (Sb₂Se₃ and Sb₂S₃)-based solar cells with a potential WS₂ electron transport layer," *Heliyon*, vol. 8, no. 12, Dec. 2022, doi: 10.1016/j.heliyon.2022.e12034.
- [8] K. M. McCreary, A. T. Hanbicki, G. G. Jernigan, J. C. Culbertson, and B. T. Jonker, "Synthesis of Large-Area WS₂ monolayers with Exceptional Photoluminescence," *Sci Rep*, vol. 6, Jan. 2016, doi: 10.1038/srep19159.
- [9] S. K. . Soni, *ICE3-2020: International Conference on Electrical and Electronics Engineering : February 14-15, 2020.* [IEEE], 2020.
- [10] J. Luis Miró-Zárate, F. Cervantes-Sodi, M. Carlos Elias-Espinosa, S. García-Trujillo, and C. J. Diliegros-Godines, "WS₂ Monolayer Integration in a FAPbI₃-based Heterostructure."
- [11] X. He, Y. Iwamoto, T. Kaneko, and T. Kato, "Fabrication of near-invisible solar cell with monolayer WS₂," *Sci Rep*, vol. 12, no. 1, Dec. 2022, doi: 10.1038/s41598-022-15352-x.
- [12] Z. He *et al.*, "Revealing Defect-State Photoluminescence in Monolayer WS₂ by Cryogenic Laser Processing."
- [13] W. Ahmed, L. Yang, U. Zahoor, and F. Wang, "Oxidation and defects in WS₂ and WSe₂: The first-principle analysis of their monolayer and bulk structures," *Journal of Physics and Chemistry of Solids*, vol. 204, Sep. 2025, doi: 10.1016/j.jpcs.2025.112775.
- [14] J. W. Wei, Z. W. Ma, H. Zeng, Z. Y. Wang, Q. Wei, and P. Peng, "Electronic and optical properties of vacancy-doped WS₂ monolayers," *AIP Adv*, vol. 2, no. 4, Dec. 2012, doi: 10.1063/1.4768261.
- [15] I. W. W. Sara, "Kalkulasi Numerik Rapat Keadaan Ws₂ Monolayer Dengan Pendekatan Ikatan Kuat Menggunakan Metode Perambatan Waktu," *Jurnal Pendidikan Fisika Undiksha*, vol. 14, no. 3, p. 541, Dec. 2024.
- [16] Q. Luan, C. L. Yang, M. S. Wang, and X. G. Ma, "First-principles study on the electronic and optical properties of WS₂ and MoS₂ monolayers," *Chinese Journal of Physics*, 2017, doi: 10.1016/j.cjph.2017.08.011.



-
- [17] M. G. Bianchi, F. Risplendi, M. Re Fiorentin, and G. Cicero, "Engineering the Electrical and Optical Properties of WS₂ Monolayers via Defect Control," Jan. 26, 2024, *John Wiley and Sons Inc.* doi: 10.1002/advs.202305162.
- [18] S. Salehi and A. Saffarzadeh, "Atomic defect states in monolayers of MoS₂ and WS₂," *Surf Sci*, vol. 651, pp. 215–221, Sep. 2016, doi: 10.1016/j.susc.2016.05.003.
- [19] A. Nakata, D. R. Bowler, and T. Miyazaki, "Large-Scale DFT Methods for Calculations of Materials with Complex Structures."
- [20] K. F. Garrity and K. Choudhary, "Fast and Accurate Prediction of Material Properties with Three-Body Tight-Binding Model for the Periodic Table," Dec. 2021, doi: 10.1103/PhysRevMaterials.7.044603.
- [21] S. Yuan, R. Roldán, M. I. Katsnelson, and F. Guinea, "Effect of point defects on the optical and transport properties of MoS₂ and WS₂," *Phys Rev B Condens Matter Mater Phys*, vol. 90, no. 4, Jul. 2014, doi: 10.1103/PhysRevB.90.041402.
- [22] M. Luo, S. Y. Hao, and Y. T. Ling, "Ab initio study of electronic and magnetic properties in Ni-doped WS₂ monolayer," *AIP Adv*, vol. 6, no. 8, Aug. 2016, doi: 10.1063/1.4961468.
- [23] S. Mathew, A. R. Abraham, S. Chintalapati, S. Sarkar, B. Joseph, and T. Venkatesan, "Temperature dependent structural evolution of wse₂: A synchrotron x-ray diffraction study," *Condens Matter*, vol. 5, no. 4, pp. 1–9, Dec. 2020, doi: 10.3390/condmat5040076.
- [24] Y. Guan, H. Yao, H. Zhan, H. Wang, Y. Zhou, and J. Kang, "Optoelectronic properties and strain regulation of the 2D WS₂/ZnO van der Waals heterostructure," *RSC Adv*, vol. 11, no. 23, pp. 14085–14092, Apr. 2021, doi: 10.1039/d1ra01877a.
- [25] R. Roldán, M. P. López-Sancho, E. Cappelluti, J. A. Silva-Guillén, P. Ordejón, and F. Guinea, "Momentum dependence of spin-orbit interaction effects in single-layer and multi-layer transition metal dichalcogenides," Jan. 2014, doi: 10.1088/2053-1583/1/3/034003.
- [26] A. T. Paxton, *An introduction to the tight binding approximation—implementation by diagonalisation. NIC Series*, vol. 42. John von Neumann-Institut für Computing, 2009.
- [27] R. Roldán, M. P. López-Sancho, F. Guinea, E. Cappelluti, J. A. Silva-Guillén, and P. Ordejón, "Momentum dependence of spin-orbit interaction effects in single-layer and multi-layer transition metal dichalcogenides," *2d Mater*, 2014, doi: 10.1088/2053-1583/1/3/034003.
- [28] Y. Li, Z. Zhan, X. Kuang, Y. Li, and S. Yuan, "TBPLaS: a Tight-Binding Package for Large-scale Simulation," Sep. 2022, [Online]. Available: <http://arxiv.org/abs/2209.00806>



-
- [29] S. Yuan, H. De Raedt, and M. I. Katsnelson, "Modeling electronic structure and transport properties of graphene with resonant scattering centers," Jul. 2010, doi: 10.1103/PhysRevB.82.115448.
- [30] R. Schneider, H. Gharibnejad, and B. I. Schneider, "ITVOLT: An Iterative Solver for the Time-Dependent Schrödinger Equation," Oct. 2022, doi: 10.1016/j.cpc.2023.108780.
- [31] F. Wooten, "OPTICAL PROPERTIES OF SOLIDS," 1972.
- [32] S. Yuan, H. De Raedt, and M. I. Katsnelson, "Modeling electronic structure and transport properties of graphene with resonant scattering centers," *Phys Rev B Condens Matter Mater Phys*, vol. 82, no. 11, Sep. 2010, doi: 10.1103/PhysRevB.82.115448.
- [33] K. Aly, "Adjusting the relation between the imaginary part of the dielectric constant and the wavelength," *Physica B Condens Matter*, vol. 655, Apr. 2023, doi: 10.1016/j.physb.2023.414723.
- [34] N. Tuan Hung, A. R. T Nugraha, and R. Saito, "Quantum ESPRESSO Course for Solid-State Physics.indd."
- [35] X. Wang, F. Wang, Y. Sang, and H. Liu, "Full-spectrum solar-light-activated photocatalysts for light–chemical energy conversion," *Adv Energy Mater*, vol. 7, no. 23, Dec. 2017, doi: 10.1002/aenm.201700473.
- [36] D. Svintsov and Z. Devizorova, "Photon drag at the junction between metal and 2d semiconductor," Nov. 2024, doi: 10.1134/S0021364024604688.
- [37] X. Zhang and Z. Sun, "Effects of vacancy structural defects on the thermal conductivity of silicon thin films," *Journal of Semiconductors*, vol. 32, no. 5, May 2011, doi: 10.1088/1674-4926/32/5/053002.
- [38] J. Wang *et al.*, "Improving the reflectance and color contrasts of phase-change materials by vacancy reduction for optical-storage and display applications," *Opt Lett*, vol. 45, no. 1, p. 244, Jan. 2020, doi: 10.1364/OL.45.000244.
- [39] L. Prangnell, "Visible Light-Based Human Visual System Conceptual Model."